How Does the Particle Density Affect the Electrochemical Behavior of Gold Nanoparticle Assembly?

3 AUTHORS, INCLUDING:

Peng Diao
Beihang University(BUAA)
69 PUBLICATIONS **1,738** CITATIONS

How Does the Particle Density Affect the Electrochemical Behavior of Gold Nanoparticle Assembly?

Peng Diao,*,† Min Guo,*,‡ and Qi Zhang†

Department of Applied Chemistry, School of Materials Science and Engineering, Beijing University of Aeronautics and Astronautics, and Department of Physical Chemistry, University of Science and Technology Beijing, Beijing 100083, People's Republic of China

Gold nanoparticles assembled on conducting substrates by organic films are usually employed as new-type electrodes, which show great potential in electrochemistry. The purpose of this work is to clarify how the particle density influences the electrochemical behavior of nanoparticle assembly electrodes. In this work, gold nanoparticles (AuNPs) are immobilized on gold substrates by using 11-amino-1-undecanethiol (AUT) as bridging molecules, and the resulting Au/AUT/AuNPs are characterized by scanning electron microscopy (SEM) and electrochemical methods. It is found that the particle density has a great influence on the cyclic voltammetric (CV) behaviors of Au/AUT/AuNP electrodes. Briefly, the higher the particle density, the more reversible the CV behavior of AuNP assembly electrodes. The particle-density-dependent CV behavior is attributed to the variations in the number of electron tunneling channels between AuNPs and the underlying gold substrates as a function of particle density. A higher particle density results in more tunneling channels and then a smaller apparent tunneling resistance, $R_{t(app)}$. The $R_{t(app)}$ of the Au/AUT/AuNPs reflects the tunneling probability across the insulating organic layer that immobilizes the AuNPs on the substrates. It is demonstrated that the influence of $R_{t(app)}$ on the CV behavior of the Au/AUT/AuNP electrode is quite similar to that of the solution resistance. The theory of solution resistance can be successfully used to calculate $R_{t(app)}$ and the particle density. The calculated particle densities are in reasonable agreement with those obtained from SEM measurements. It is also shown that the effect of tunneling on the CV behavior of Au/AUT/AuNPs can be greatly reduced by using electrodes with a high particle density and slow potential sweep. Our work provides solid evidence that the tunneling process across the bridging molecules has a great effect on the electrochemical behaviors of nanoparticle array electrodes. As a result, when assembled nanoparticle electrodes are used in electroanalytical works, the tunneling process must be taken into account, especially for the electrode with a relatively lower particle density.

Introduction

The ability to construct well-defined nano- and submicrostructures by "bottom up" approaches is a major goal in the field of nanoscale science and technology. In recent years, nanoparticles have been the subject of numerous investigations concerning nanoconstruction;[1–9] the origin of the extensive interests is that nanoparticles are widely accepted as ideal building blocks due to the ease of preparation and the accurate control over the particle size and shape.[10–15] Assembling nanoparticles into one-, two- and three-dimensional architectures is one of the most extensively studied bottom up approaches to building functional nanostructures on solid substrates.[1,6–9,15–31] Usually the substrate surfaces are chemically pretreated to produce functional groups that have a strong interaction with nanoparticles.[1,7,8,16,20,21] Of particular significance are electrically conducting substrates, enabling the nanoparticle arrays to be utilized, for instance, in electrochemical systems.[20–31] Several surface derivatization schemes have been developed along these lines, employing self-assembled monolayers (SAMs) with special terminating groups, polymers, or sol–gel host matrixes.[16,20–33] The obtained nanoparticle assemblies have shown great potential in electroanalysis.[21–24,28,29]

Many applications of nanoarchitectures require chemical, optical, or biological signals to be transformed into electrical signals that are readable to modern electronic equipment. Therefore, the ability to allow electron communication between the nanoparticles and the underlying substrates is essential to these applications. However, as mentioned above, the nanoscale building blocks are usually immobilized on a substrate via a thin layer of insulating organic film, such as SAMs or polymers.[16,20,25–33] These insulating films act as energy barriers and greatly reduce the electron-transfer rate through the films. It has been demonstrated that, for compact and pinhole-free SAMs, the only way for charge transfer is electron tunneling through the SAMs and that the tunneling barrier increases exponentially with the film thickness.[34–40] As a result, the electrodes coated with long-chain SAMs are almost totally blocked even to the outer-sphere redox couples in the potential windows within which bare electrodes show reversible behaviors.[34,36,38] Surprisingly, after the conductive nanoscale building blocks, such as gold nanoparticles (AuNPs) and shortened carbon nanotubes, are attached to the film-coated electrodes, reversible or quasi-reversible electron transfer returns,[20,26–28,41–43]

* To whom correspondence should be addressed. (P.D.) Phone and fax: 86-10-8231-6841. E-mail: pdiao@buaa.edu.cn. (M.G.) Phone: 86-10-6233-4926. E-mail: guomin@metall.ustb.edu.cn.
† Beijing University of Aeronautics and Astronautics.
‡ University of Science and Technology Beijing.

Electrochemical Behavior of AuNP Assembly

J. Phys. Chem. C, Vol. 112, No. 17, 2008 **7037**

though the insulating thin film still lies between the nanoscale building blocks and the underlying electrodes. It is believed that the immobilized conductive building blocks serve as an electron relay station and greatly facilitate electron tunneling through the organic film.[42]

Furthermore, the particle density is found to have a great effect on the electrochemical behavior of the nanoparticle-modified electrodes.[26−28,42] Bharathi et al.[26] first reported that, for the AuNP-modified gold electrodes, the peak current in cyclic voltammetric (CV) curves increased and the peak-to-peak potential separation decreased with increasing particle density. This means that the electron-transfer kinetics could be tuned by varying the particle density. A longer assembly time resulted in a higher particle density and then a faster electron-transfer rate. However, they did not present a mechanism to explain the particle-density-dependent electrochemical behavior.[26] Wang et al.[28] prepared a nanoparticle-modified electrode by anchoring AuNPs onto an indium tin oxide (ITO) substrate using a (3-mercaptopropyl)trimethoxysilane SAM as the linking layer. They demonstrated that the AuNP-modified ITO electrode exhibited greatly enhanced sensitivity relative to macroelectrodes in electroanalytical measurements. Similar to the work of Bharathi et al.,[26] they also found that a higher particle density led to faster electron-transfer kinetics.[28] They ascribed the effect of the particle density to the nonlinear diffusion behavior of the unevenly dispersed nanoparticle arrays.[28] We[41,42] and others[43−47] reported the assembly of carbon nanotubes onto SAM-coated gold electrodes and found that the nanotubes greatly improved the electron communication between the gold electrode and redox species either in solution or bonded to the nanotubes. We also showed that the electron-transfer barrier could be greatly reduced by increasing the nanotube density.[42] According to the above-mentioned literature, it can be concluded that the particle density can greatly influence the sensitivity and the precision of electrochemical sensors based on nanoparticle assemblies.

For AuNP-modified electrodes, the electron communication process involves two steps: (i) electron transfer between the redox couple and the tethered AuNPs, (ii) electron tunneling through the linking organic layer between AuNPs and the underlying electrode. As the particle density varies, the number of routes for tunneling changes accordingly, and hence, the apparent electron-transfer rate changes. However, this is not taken into account in most studies concerning the electrochemistry of a nanoparticle assembly, though it may be critical to the application of AuNP assemblies in electroanalysis. The purpose of this work is to clarify how the particle density influences the electrochemical behavior of AuNP assembly electrodes. We will show that the electron tunneling is the key step influencing the whole electron-transfer kinetics.

Experimental Section

Chemicals. 11-Amino-1-undecanethiol (AUT) was purchased from Dojindo Co. (Japan). $Ru(NH_3)_6Cl_3$ was obtained from Alfa Aesar (a Johnson Matthey Co.). Both were of analytical grade and used as received. Other chemicals were of analytical grade. The AUT solution was prepared by dissolving AUT in absolute ethanol, and its final concentration was 1 mM.

Preparation of the AUT Monolayer on Gold. Gold substrates were prepared on Si wafers by sputtering with 150 nm Au (99.99%). A 10 nm Cr layer was deposited prior to Au deposition to improve adhesion to the Si wafer. Prior to use, the gold substrates were cleaned in "piranha" solution (1:3 30% H_2O_2/concentrated H_2SO_4, volume ratio) at 90 °C for 10 min

followed by rinsing with copious water and absolute ethanol, successively. *Caution: piranha solution reacts violently with organic material!* AUT monolayers were formed by immersing gold substrates in 1 mM AUT solution for 24 h. Prior to surface modification with AuNPs, the monolayer-coated gold substrates (noted as Au/AUT) were washed with ethanol to rinse off residual AUT molecules and then dried in a stream of high-purity N_2.

Assembly of AuNPs onto Gold Substrates. Gold colloids were prepared by the Frens method.[10] Briefly, an aqueous solution of sodium citrate (1.75 mL, 1 wt %) was added to a boiling $HAuCl_4$ (50 mL, 2.5×10^{-4} M) solution under vigorous stirring. The average gold particle size, determined by transmission electron microscopy (TEM; Hitachi-9000, Japan), was about 13 nm. Before use, the pH of the colloid solution was adjusted to 4.5. The AUT-SAM-coated gold substrates were immersed in the gold colloid for the required time to form a nanoparticle assembly. After the immersion, the resulting AuNP-modified substrates (noted as Au/AUT/AuNPs) were rinsed with copious water.

Electrochemical Measurements. Cyclic voltammetric measurements were performed on a CHI660A electrochemical workstation (CH Instruments Co.). All CV experiments were carried out in a conventional three-electrode cell at room temperature. For all working electrodes, the geometric area exposed to solution is 0.26 cm^2. A saturated calomel electrode (SCE) and a Pt foil were employed as reference and counter electrodes, respectively. All potentials are reported with respect to SCE.

Scanning Electron Microscopic (SEM) Characterization. The micrographs of assembled nanoparticle monolayers were obtained on a Philips FEI XL30 SFEG scanning electron microscope with an accelerating potential of 10 kV.

X-ray Photoelectron Spectroscopic (XPS) Characterization. After the formation of the AUT SAM, the gold substrate was put into the chamber of the XPS instrument. The XPS measurements were carried out on an AXIS-Ultra instrument from Kratos Analytical using monochromatic Al Kα radiation (225 W, 15 mA, 15 kV) and low-energy electron flooding for charge compensation. To compensate for the surface charge effects, all binding energies were calibrated using the C(1s) hydrocarbon peak at 284.80 eV.

Results and Discussion

Characterization of Amino-Terminated SAMs and AuNP Assemblies Prepared on Gold Substrates. The AUT molecule is terminated with an amino group, and the nitrogen atom in the amino group can be used to determine the existence of AUT molecules. Therefore, the XPS measurements were carried out to characterize the AUT-monolayer-coated gold substrates. For the Au/AUT electrode, a N(1s) peak, which arises from the amino groups of the AUT molecules, can be clearly observed at a binding energy of 399.3 eV in the XPS spectrum (data not shown), whereas the bare gold substrate shows no peak in the same position. This clearly indicates the presence of AUT molecules on the gold surface. Studies on the packing density of organosulfur SAMs have shown that −CH$_3$-terminated alkanethiol molecules form densely packed SAMs on the gold surface, which can block the charge transfer between the underlying gold electrode and the electroactive species in solution.[34,36−38] In this work, the AUT SAM was prepared from an AUT solution of absolute ethanol, in which the −NH$_2$ group is not positively charged due to the lack of free protons in solution. The electroneutral −NH$_2$ group rules out the possibility
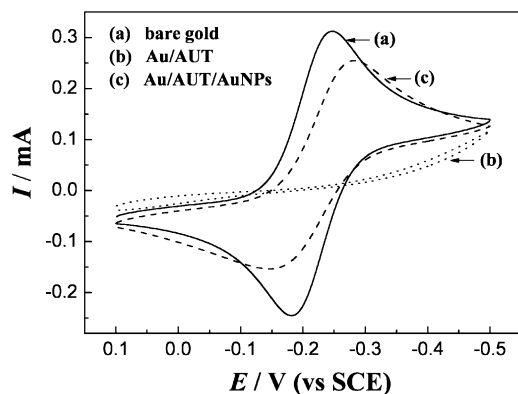
Figure 1. Cyclic voltammograms of bare gold (a), Au/AUT (b), and Au/AUT/AuNPs (c) in 5 mM Ru(NH₃)₆Cl₃ solution with 1 M KCl as the supporting electrolyte. The Au/AUT/AuNP electrode was prepared by immersing Au/AUT in gold colloid solution for 20 min. The scan rate was 0.1 V·s⁻¹.

that there is a strong electrostatic repulsion between AUT molecules, which may result in a loosely packed AUT SAM. On the contrary, the uncharged −NH₂ group allows the formation of hydrogen bonds between adjacent AUT molecules and then may lead to a higher packing density, since it has been demonstrated that hydrogen bonds between the terminal groups of the SAM help improve the packing density of the SAM.[36,37] Electrochemical measurements were carried out in this work to see whether the AUT molecules form a densely packed monolayer. As is well-known, the −NH₂ group is protonated in a neutral aqueous solution and the resulting positively charged −NH₃⁺ repels the cations and attracts the anions. As a result, a densely packed AUT monolayer blocks the electron transfer between the gold substrate and the positively charged electro-active species in solution, such as Ru(NH₃)₆³⁺.[48] Parts a and b of Figure 1 show the cyclic voltammograms of bare and AUT-coated gold electrodes in Ru(NH₃)₆³⁺ solution, respectively. The blocking behavior of the Au/AUT electrode indicates that a dense AUT monolayer is formed on the surface of the gold substrate.

The isoelectric point of the gold colloids prepared by the aqueous reduction of HAuCl₄ by sodium citrate at reflux is about 2.[49] As a result, the gold nanoparticles are negatively charged due to the adsorption of anions when the pH value of the colloid solution was adjusted to 4.5. Upon the immersion of Au/AUT in gold colloid, the strong electrostatic interaction between the positively charged AUT monolayer and the negatively charged AuNPs leads to the immobilization of AuNPs on the AUT-modified electrodes.[21,25,32] Figure 1c shows the CV curve of the resulting Au/AUT/AuNP electrode in 5 mM Ru(NH₃)₆Cl₃ solution. It is interesting to note that the disappeared redox peaks reappear after the assembly of AuNPs on the blocked Au/AUT electrode. This is in good agreement with other AuNP assembly systems in which different linking layers or redox probes were employed.[20,24,26,28] There are two possibilities for the return of redox peaks: (1) The electrostatic attraction between the −NH₃⁺ group and the negatively charged AuNP leads to the rearrangement of the AUT chains and then creates large numbers of pinholes in the AUT monolayer. (2) The assembled AuNPs have good electron communications with the underlying gold electrode and then act as nanoelectrode arrays. The first possibility was ruled out by a previously conducted experiment, in which we demonstrated that the electrostatic attraction between the positively charged −NH₃⁺ group and the negatively charged −COO⁻ group has little effect on the electrochemical behavior of AUT-SAM-coated gold electrodes.[41] Therefore, the return

of redox currents upon the immersion of Au/AUT in gold colloid solution indicates that AuNPs are anchored on the surface of the AUT monolayer and act as nanoelectrodes. These nano-electrodes greatly enhance the electron-transfer rate between Ru(NH₃)₆³⁺/²⁺ and the AUT-monolayer-coated gold substrate. It has been demonstrated that electron tunneling across the bridging SAMs is the charge-transfer mechanism.[35,50−57] We also found that the CV behaviors of the AuNP assembly electrode show a dependence on the length of the bridging molecules. At constant particle density (constant assembly time in gold colloid), longer bridging molecules lead to smaller peak currents and larger peak-to-peak potential separations. Considering that the purpose of this work is to demonstrate how and why the particle density influences the electrochemical behavior of the AuNP assembly, we fixed the tunneling distance by using AUT as the only bridging molecule because a constant tunneling distance can greatly simplify the problem and makes the quantitative comparison among samples with different particle densities possible.

SEM characterization was performed to provide direct evidence that AuNPs are immobilized on the gold substrates. Parts a−e of Figure 2 show the SEM images of Au/AUT/AuNPs prepared by immersing Au/AUT in gold colloid solution for different times. It can be clearly seen from Figure 2 that a monodispersed AuNP assembly with uniform particle density is obtained for all samples. The closely located but isolated AuNPs at high particle coverage indicate a strong repulsive force between nanoparticles, which prevents AuNPs from forming two- and three-dimensional aggregates. This is in sharp contrast with AuNP films prepared by electrophoretic deposition, in which the attraction between AuNPs leads to a close-packed two-dimensional structure.[58] Moreover, our work agrees well with the self-assembled AuNP submonolayer prepared on polymerized organosilane films,[8,28] in which covalent bonds are formed between the terminal sulfhydryl groups of the orga-nosilane film and the surface of AuNPs. Compared to the AuNP submonolayer prepared on an organosilane film,[8,28] the AuNP assembly obtained in this work has a superior uniformness in particle density. We believe this is due to the fact that AUT molecules form an even monolayer on the surface of the gold substrate, whereas the uneven polymerization of organosilane leads to the formation of film patches on the solid surface.[8] From the above discussion, it can be concluded that the assembly method use in this work is reliable and applicable for the preparation of a uniform and monodispersed AuNP submono-layer on gold. We will show in the later sections that the uniform particle density is very important to study the electrochemical behavior of AuNP assemblies.

As can be seen in Figure 2a−e, the particle coverage on Au/AUT is strongly dependent on the incubation duration in gold colloid solution, especially in the initial incubation stage. The plot of the particle density versus immersion time is shown in Figure 2f (solid circles), which demonstrates two distinct assembly steps: an initial rapid step that lasts less than 1 h and a slow step that takes several hours or longer. Within the rapid assembly stage (immersion time <1 h), the particle density, N, can be nicely predicted by the equation $N = (4.54 \times 10^9)t^{1/2}$ (the solid line in Figure 2f), where t is in minutes. The $t^{1/2}$ relationship essentially reflects that the diffusion of AuNPs is the rate-determining process, while for the samples with a longer assembly time, the particle density deviates negatively from the $t^{1/2}$ dependence, which is most likely due to the enhanced electrostatic repulsion between AuNPs. All these experimental results are in good agreement with kinetic studies performed
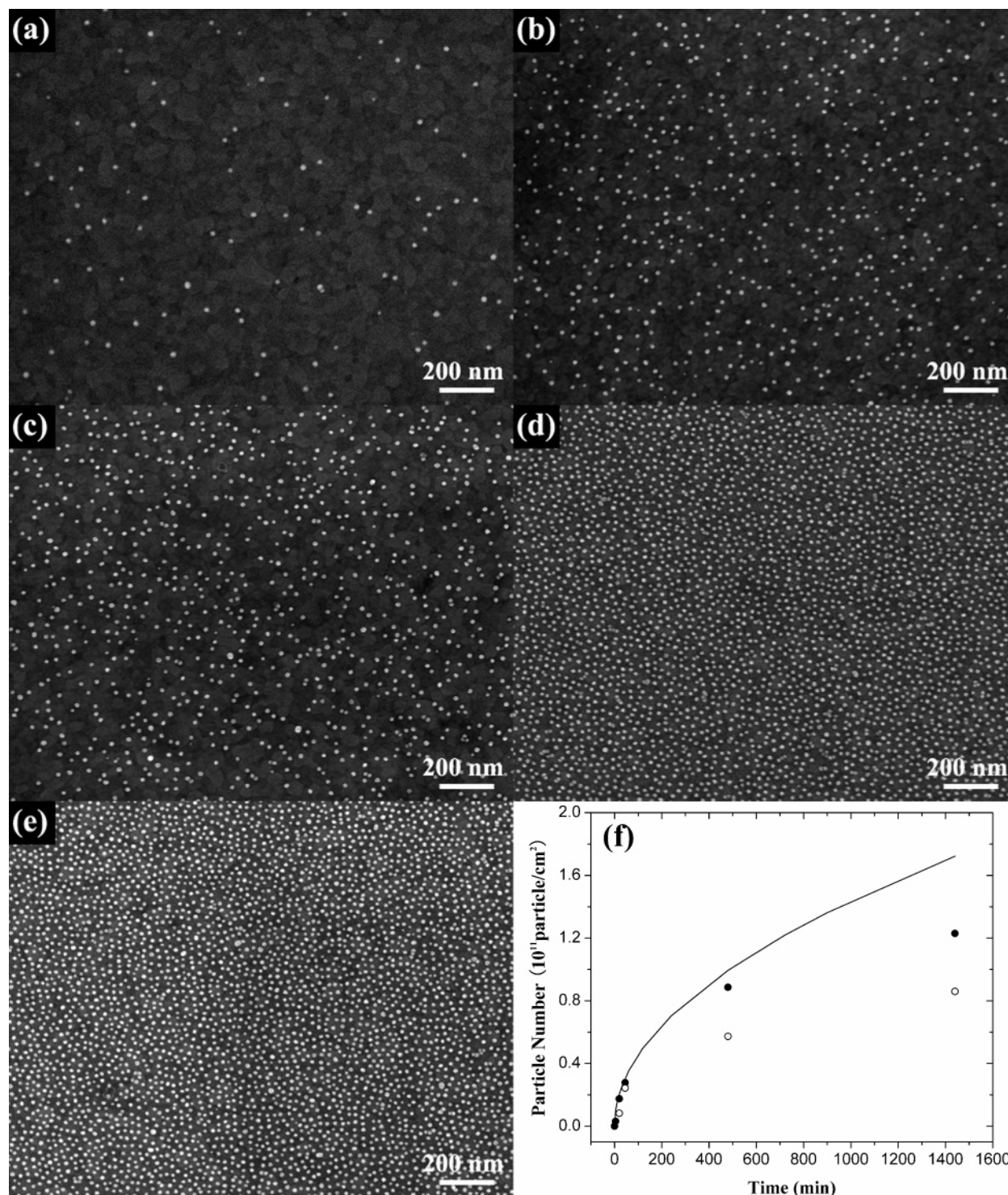
Figure 2. SEM images of Au/AUT/AuNPs with different assembly times in gold colloid solution: (a) 5 min, (b) 20 min, (c) 45 min, (d) 480 min, and (e) 1440 min. (f) Particle density vs immersion time in gold colloid. The solid circles represent the data obtained by SEM, while the open circles represent the particle densities obtained by the electrochemical method. The solid line shows the $t^{1/2}$ dependence of the particle density N: $N = (4.54 \times 10^9)t^{1/2}$ (t is in minutes), where the coefficient is obtained from a nonlinear least-squares fit to the data points within the first hour.

previously.[8,28,32] When the immersion time in gold colloid exceeds 1440 min, the particle density remains almost unchanged within the measurement error range. Therefore, the particle density of the sample with a 1440 min immersion time can be used to describe the saturation coverage, which is counted from Figure 2e as 1.23×10^{11} particles·cm^{-2}. The $t^{1/2}$ dependence in the early assembly stage suggests that monodispersed AuNP assemblies with a well-controlled particle density can be obtained by simply varying the immersion time in gold

colloid. However, to obtain a high density, a much longer immersion time is required due to the significantly negative deviation from $t^{1/2}$ dependence.

Effect of the Particle Density on the Electrochemical Behavior of the Au/AUT/AuNP Electrode. Figure 3 shows the CV curves of four Au/AUT/AuNP electrodes in Ru(NH$_3$)$_6$$^{3+}$ solution. The assembly time in gold colloid for these electrodes is 5, 20, 45, and 1440 min. As shown in Figure 3, only the sample with a 5 min immersion exhibits a CV curve charac-
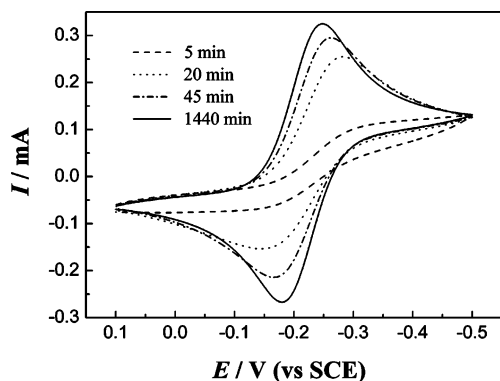
Figure 3. Cyclic voltammograms of Au/AUT/AuNP electrodes in 5 mM Ru(NH₃)₆Cl₃ solution with 1 M KCl as the supporting electrolyte. The Au/AUT/AuNP electrodes were prepared by immersing Au/AUT in gold colloid for 5, 20, 45, and 1440 min, respectively. The scan rate was 0.1 V·s⁻¹.
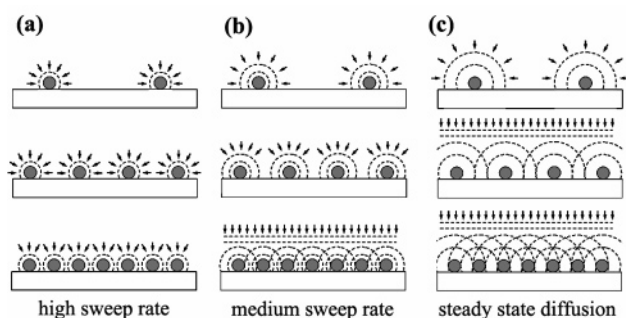

Figure 4. Schematic representation of the diffusion models of nanoparticle electrode arrays under different potential sweep rates: (a) high sweep rate under which the diffusion layer thickness is much smaller than half the average distance between adjacent particles, (b) medium sweep rate under which the diffusion layers of adjacent particles overlap for a high particle density, (c) very low sweep rate under which steady-state diffusion is reached for all samples.

teristic of a microelectrode, while the others demonstrate CV features of a macroelectrode. In addition, for the Au/AUT/AuNPs with an immersion time ≥20 min, the peak current increases and the peak-to-peak potential separation decreases as the immersion time in gold colloid is increased. These observations are in good agreement with AuNP assemblies prepared on gold-supported organosilane films[26−28] and single-wall carbon nanotube assemblies prepared on AUT-coated gold substrates.[42]

To fully understand these observations, we first need to discuss the CV behavior of a reversible redox couple on a microelectrode array. As demonstrated previously,[59−61] the CV behavior of a reversible redox couple on a microelectrode array is determined by three factors: the diameter of individual microelectrodes, the average distance between adjacent microelectrodes, and the diffusion layer thickness. Among these factors, the diffusion layer thickness is determined by the time scale of the experiments, in the case of CV measurements, determined by the potential sweep rate. When the potential sweep rate is high enough, the diffusion layer thickness is smaller than half the separation between adjacent AuNPs even at high particle densities. As a result, a CV behavior characteristic of microelectrodes is expected for all samples, as shown in Figure 4a. When the sweep rate is lowered, two different CV behaviors may be present depending on the particle density, as shown in Figure 4b. At high particle densities, the diffusion layer thickness is larger than half the distances between adjacent

particles, leading to the formation of a single larger field due to the merging of individual diffusion layers. Under this condition, the nanoparticle assembly exhibits a linear diffusion behavior of a macroelectrode and has an area equal to the geometric area of the substrate (see the bottom scheme in Figure 4b).[62] However, at low particle densities with average particle separation larger than the sum of the thickness of two individual diffusion layers, microelectrode-type CV features are expected, as shown in the upper two schemes in Figure 4b. When the sweep rate is low enough that all individual particles exhibit steady-state diffusion, only the sparsely populated samples will show steady-state microelectrode-type CV behavior, as illustrated in the top scheme in Figure 4c. At high particle densities that ensure the overlap of individual diffusion layers, linear diffusion of a macroelectrode is expected. Under this condition, the effective electrode area is the projected area of the diffusion layer.[62] Therefore, the effective area of the nanoparticle assembly does not change even though the particle density is further increased, as shown in the lower two schemes in Figure 4c.

Which of the above-mentioned cases fits into the gold nanoparticle assembly electrode used in this work? To answer this question, we first need to determine the potential sweep rate under which the individual nanoparticle electrode shows steady-state diffusion behavior. It has been demonstrated that, for an ultramicroelectrode, the voltammogram will be a steady-state response if the following equation is satisfied:[62]

$$v \ll RTD/nFr_0{}^2 \qquad (1)$$

where v is the potential sweep rate, D is the diffusion coefficient of the redox probe, r_0 is the radius of the electrode, and R, T, n, and F have their usual significance. In our experiments, $r_0 = 6.5$ nm, $n = 1$, $T = 298$ K, and the diffusion coefficient of Ru(NH₃)₆³⁺ is 7.1×10^{-6} cm²·s⁻¹.[63] $RTD/nFr_0{}^2$ is calculated to be 4.3×10^5 V·s⁻¹, which is much larger than the maximum value of v used in this work. Therefore, on the basis of eq 1, each individual AuNP exhibits a steady-state diffusion behavior in our CV experiments. Under this condition, the particle density (the average distance between adjacent AuNPs) determines whether the individual AuNPs exhibit independent CV behaviors. It has been demonstrated that the diffusion layer will not overlap if the following equation holds:[28,64]

$$d/r_0 > 12 \qquad (2)$$

where d is the average center-to-center distance between adjacent particles. Upon knowing the particle number N per square centimeter (particle density), d can be calculated from the following equation (see the Supporting Information):

$$d = (1/N)^{1/2} \qquad (3)$$

The calculation results are shown in Table 1, from which we note that $d/r_0 > 12$ holds only for the sample with a 5 min assembly time, suggesting that a microelectrode-type CV behavior will be expected. As for the Au/AUT/AuNPs with a longer assembly period (≥20 min), the values of d/r_0 are smaller than 12, indicating that macroelectrode-type CV behaviors will be observed on these samples. All these theoretical predictions are in good agreement with experimental results shown in Figure 3, in which the 5 min sample exhibits a limiting current characteristic of microelectrodes, whereas the other samples show typical CV behavior of macroelectrodes. This means that, for the Au/AUT/AuNPs with an assembly time ≥20 min, the

TABLE 1: Particle Density and Interparticle Center-to-Center Distance as a Function of the Assembly Time in Gold Colloid Solution

assembly time (min)	N (particles·cm^{-2})	d (nm)	$d/r_0{}^a$
5	3.09×10^9	180	27.7
20	1.75×10^{10}	76	11.6
45	2.78×10^{10}	60	9.2
480	8.86×10^{10}	34	5.2
1440	1.23×10^{11}	29	4.5

^{a} r_0 is the radius of the gold nanoparticle. In this work r_0 is 6.5 nm.

diffusion layer of individual particles merges into a larger uniform field and the linear steady-state diffusion dominates the mass-transfer process, as shown schematically in the lower two schemes in Figure 4c.

However, there are observations in Figure 3 that cannot be well explained by the theory discussed above. As we have mentioned, a high particle density leads to a uniform diffusion field, and the effective area of the Au/AUT/AuNP electrode is the projected area of the diffusion layer, which does not change with further increasing particle density. In other words, the CV behavior of the Au/AUT/AuNPs with an assembly time ≥ 20 min should be the same regardless of the particle density. However, Figure 3 shows that both the peak potential and the peak current change as a function of the particle density. This phenomenon was also observed previously[26,28] and was ascribed to the nonlinear diffusion caused by uneven dispersion of AuNPs.[28] However, this explanation does not suit the case in our experiments because the AuNPs are uniformly dispersed on the substrates, as can be clearly seen in Figure 2a−e. Therefore, there must be some other reasons for the particle-density-dependent CV behavior. Three possible reasons might be responsible for the observed CV behavior: (1) A high particle density enhances the particle−particle electron-transfer rate and then greatly improves the electron communication between AuNPs and the underlying electrode. (2) A high particle density helps improve the electron-transfer rate between Ru(NH$_3$)$_6{}^{3+}$ and the individual AuNPs. (3) The electron tunneling through the AUT monolayer is the rate-determining step for the whole electrode process, and a higher particle density results in more tunneling channels and then significantly increases the electron-transfer kinetics.

It is clear from Figure 2e that, for the AuNP assembly with the highest particle density, the average distance between adjacent particles is at least 10−20 nm, which is too large for electrons to tunnel through. Therefore, the first possibility can be ruled out. As for the second possibility, the electron communication rate between Ru(NH$_3$)$_6{}^{3+}$ and the individual AuNPs is governed by factors such as the surface states of the AuNPs and the concentration and the nature of the electroactive species. However, none of these factors are dependent on the particle density. Moreover, it has been clearly demonstrated that the electron-transfer rate between Ru(NH$_3$)$_6{}^{3+}$ and nanoscale electrodes is extremely fast.[65] Therefore, it can be safely concluded that the particle density has little effect on the electron-transfer rate between Ru(NH$_3$)$_6{}^{3+}$ and the gold nanoparticle.

Then only the last possibility is left. To explain this particle-density-dependent CV behavior by the tunneling model mentioned above, the overall electron-transfer process at Au/AUT/AuNPs should be carefully examined. Taking, for example, the electrochemical reduction of Ru(NH$_3$)$_6{}^{3+}$ at the Au/AUT/AuNP electrode, the electron-transfer process involves the following

two steps (see Figure 5a): (i) electron transfer from the gold substrate to the AuNPs via tunneling through the sandwiched organic film, (ii) electron transfer from the AuNP to Ru(NH$_3$)$_6{}^{3+}$ at the AuNP/solution interface, resulting in the electrochemical reduction of Ru(NH$_3$)$_6{}^{3+}$. If we assume that step i is much faster than step ii, then the influence of the first step on the CV behavior can be left out. The second step is diffusion controlled due to the extremely fast electron-transfer kinetics of the Ru(NH$_3$)$_6{}^{3+/2+}$ couple on the nanoelectrodes.[65] Therefore, a linear diffusion behavior would be expected when the particle density is high enough to ensure the overlap of individual diffusion layers. As we have discussed above, the linear diffusion leads to a constant effective area for Au/AUT/AuNPs, which is independent of the particle density. In other words, the particle density has no effect on the CV features under this condition. Therefore, step ii is not responsible for the particle-density-dependent CV behavior of Au/AUT/AuNPs, and the assumption that the effect of step i on the CV behavior can be omitted is untenable. As for the tunneling mechanism in step i, it has been demonstrated in previous works[35,50−52,57] that through bonds of molecule chains is the predominant pathway of electron tunneling. Therefore, we mean "through-bond tunneling" when we say "tunneling" in all discussions. Therefore, in step i, the electron tunneling rate is dominated by two factors: the thickness of the insulating layer and the assembly density of nanoparticles. The former governs the height of the tunneling barrier and then influences the tunneling probability of a single tunneling channel between the gold substrate and individual AuNPs, while the latter determines the number of tunneling channels on the whole Au/AUT/AuNP electrode. It is obvious that the particle density does not affect the tunneling barrier at an individual AuNP due to the constant thickness of the AUT monolayer. Therefore, we believe the number of tunneling channels, which is dominated by the number of nanoparticles per unit area, is responsible for the particle-density-dependent CV behavior.

One single electron tunneling between the gold substrate and a AuNP is an elastic and instantaneous process during which the energy of the tunneling electron is conserved. Therefore, there should be no resistance for a single electron tunneling that is accomplished instantaneously. However, for a long time duration, the tunneling resistance R_t, which is defined as the quotient of potential bias and the obtained current, is usually employed to describe the electron tunneling. In fact, R_t does not represent the real tunneling resistance, but reflects the probability of tunneling through a single molecule between the gold substrate and a AuNP. Under the same potential bias, the higher the probability of tunneling, the larger the tunneling current and then the smaller the R_t value.

The tunneling resistance through a single-molecule bridge between the gold substrate and a AuNP, R_t, can be expressed as[55,56,66]

$$R_t = R_0 \exp(\beta l) \qquad (4)$$

where R_0 is the effective contact resistance of the two separated phases, β is the electron tunneling coefficient, and l is the thickness of the barrier. Since one AuNP is linked by many AUT bridge molecules, there may be more than one tunneling channel between one AuNP and the underlying substrate. The number of tunneling channels for a single AuNP has been studied with AuNP arrays assembled on SAM-coated gold substrates by using scanning tunneling microscopy (STM).[50] Statistics based on a large amount of STM data demonstrates that, for a single AuNP, there are five possible tunneling cases
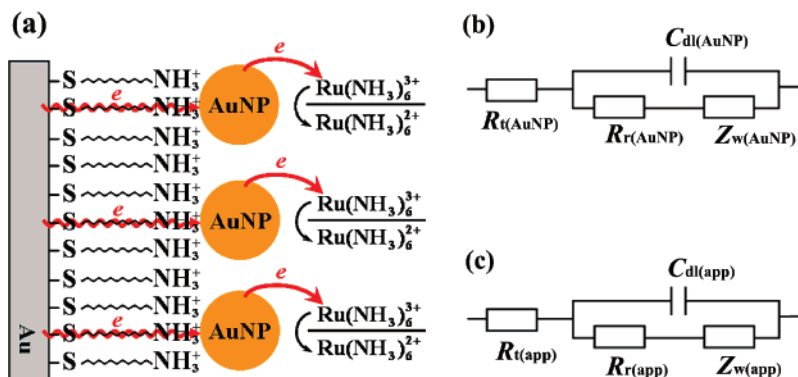
Figure 5. (a) Schematic representation of the electron transfer at a Au/AUT/AuNP electrode. (b) EQC of the electrochemical process at a single AuNP. (c) Simplified EQC of the entire AuNP assembly, which is obtained by connecting in parallel the EQCs of all immobilized AuNPs. $R_{t(AuNP)}$, $C_{dl(AuNP)}$, $R_{r(AuNP)}$, $Z_{w(AuNP)}$, and $R_{s(AuNP)}$ are the tunneling resistance, double-layer capacitance, charge-transfer resistance, and Warburg impedance at a single AuNP electrode, respectively. $R_{t(app)}$, $C_{dl(app)}$, $R_{r(app)}$, and $Z_{w(app)}$ are the apparent tunneling resistance, apparent double-layer capacitance, apparent charge-transfer resistance, and Warburg impedance at Au/AUT/AuNPs, respectively. The solution resistance is left out because it is negligible compared to the tunneling resistance.

that contain one, two, three, four, or five parallel tunneling channels. The number of tunneling channels (one, two, three, four, or five) for a specific AuNP is random and independent of the particle size. Moreover, the probability of each case is almost equal.[50] According to these results, it is easy to deduce that the average number of tunneling channels for a single AuNP is three. Therefore, it is reasonable to assume that, in our work, there are three parallel tunneling channels on average for a single AuNP. Then the tunneling resistance for a single AuNP, $R_{t(AuNP)}$, is one-third of R_t:

$$R_{t(AuNP)} = \frac{1}{3} R_t = \frac{1}{3} R_0 \exp(\beta l) \tag{5}$$

Figure 5b shows the equivalent circuits (EQCs) of the electrochemical process that takes place at a single AuNP electrode. As shown in Figure 5a, the charge-transfer processes at individual AuNPs are parallel to each other, and then the EQC for the whole Au/AUT/AuNP electrode can be obtained by connecting in parallel the EQCs of all AuNPs. Because the electrochemical surroundings are identical for all AuNPs, it is rational to assume that the corresponding elements at different AuNPs are the same in value. Therefore, the electrochemical process at Au/AUT/AuNPs can be described by a simplified EQC (Figure 5c), in which the value of each element is dependent on the particle density and the value of the corresponding element at a single AuNP. If we assume the particle density is N, the apparent tunneling resistance ($R_{t(app,nor)}$) of the Au/AUT/AuNP electrode, which is normalized by the geometric area of the electrode, is given by

$$R_{t(app,nor)} = \frac{1}{N} R_{t(AuNP)} \tag{6}$$

where $R_{t(app,nor)}$ is in $\Omega \cdot cm^2$, $R_{t(AuNP)}$ in $\Omega \cdot particle$, and N in particles$\cdot cm^{-2}$. On the basis of eq 6, the particle density can be calculated if we know $R_{t(app,nor)}$ and $R_{t(AuNP)}$. Accordingly, the theory presented in this paper to explain the particle-density-dependent CV behavior can be tested by comparing the value of N calculated from eq 6 with that obtained from SEM images.

Electrochemical Measurements of the Apparent Tunneling Resistance and the Particle Density. As shown in Figure 5c, the EQC of Au/AUT/AuNPs contains an apparent electron tunneling resistance $R_{t(app)}$ (not normalized, Ω), in series with a parallel apparent double-layer capacitance $C_{dl(app)}$, an apparent

charge-transfer resistance $R_{r(app)}$, and a Warbug impedance $Z_{w(app)}$. The charge-transfer rate of the redox couple Ru(NH$_3$)$_6^{3+/2+}$ at the nanoelectrode is extremely fast;[65] therefore, in the case that $R_{t(app)}$ is negligible, reversible CV curves with a 60 mV peak-to-peak potential separation (ΔE_p) should be observed and ΔE_p should be independent of the potential scan rate. However, Figure 3 clearly shows that ΔE_p is much larger than 60 mV, suggesting that $R_{t(app)}$ cannot be neglected. Moreover, as shown in Figure 6, CV curves at different scan rates demonstrate that ΔE_p increases with increasing potential scan rate, providing further evidence that the apparent tunneling resistance $R_{t(app)}$ must be taken into account when we discuss the CV behavior of Au/AUT/AuNP electrodes.

A careful inspection of Figure 5c reveals that the EQC is actually the same in form as that of a traditional macroelectrode. The only difference is that, for a Au/AUT/AuNP electrode, the apparent electron tunneling resistance $R_{t(app)}$ takes the place of the solution resistance. In addition, the scan-rate-dependent ΔE_p shown in Figure 6 indicates that the apparent effect of $R_{t(app)}$ on the CV behavior of the Au/AUT/AuNP electrode is similar to that of the solution resistance on the CV behavior of the bare macroelectrode. Therefore, the theory of solution resistance is employed in this work to calculate $R_{t(app)}$, as we have done in carbon nanotube array electrodes.[42] The effect of the solution resistance R_s on the CV behavior can be described by the following equation:[67,68]

$$H = \frac{(nF)^{5/2}}{(RT)^{3/2}} A\pi^{1/2} D_o^{1/2} C_o R_s v^{1/2} \tag{7}$$

where H is a dimensionless parameter that has great effects on the peak current and ΔE_p in CV curves, A is the area of the working electrode, v is the scan rate, and D_o and C_o are the diffusion coefficient and the concentration of the oxidized species, respectively. Other parameters have their usual meanings. Replacing R_s with $R_{t(app)}$ in eq 7, we obtain the dependence of H on $R_{t(app)}$:

$$H = \frac{(nF)^{5/2}}{(RT)^{3/2}} A\pi^{1/2} D_o^{1/2} C_o R_{t(app)} v^{1/2} \tag{8}$$

On the basis of eq 8, $R_{t(app)}$ can be calculated if we can obtain, from CV measurements, the values of H at different scan rates.
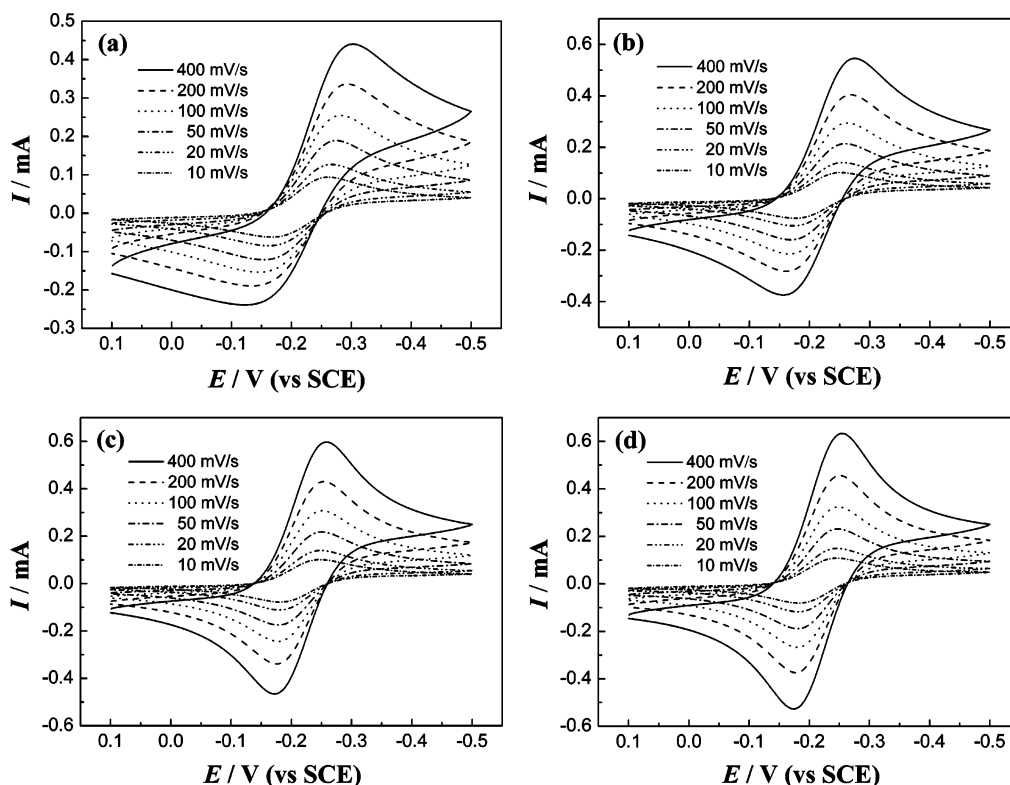
Figure 6. Typical cyclic voltammograms of Au/AUT/AuNP electrodes at different potential scan rates in 5 mM Ru(NH$_3$)$_6$Cl$_3$ solution with 1 M KCl as the supporting electrolyte. The Au/AUT/AuNP electrodes were prepared by immersing Au/AUT in gold colloid for (a) 20 min, (b) 45 min, (c) 480 min, and (d) 1440 min.

To obtain $R_{t(app)}$, we first need to establish the $H-\Delta E_p$ working curve. In this paper, the $H-\Delta E_p$ working curve was obtained at a bare Au electrode in 5 mM Ru(NH$_3$)$_6$Cl$_3$ solution with a precision decade resistance box connected between the potentiostat and the bare gold working electrode. The given resistance shared part of the potential that was applied to the electrode and then took the role of solution resistance. The CV curves with different given resistances at scan rates of 50, 100, and 200 mV·s^{-1} are shown in parts a–c, respectively, of Figure 7. The dependence of the peak current i_p and peak potential separation ΔE_p on the given resistance is in good line with that predicted by solution resistance theory.[67,68] For a constant scan rate, the value of ΔE_p at different resistances can be obtained from Figure 7a–c. The corresponding H can be calculated by taking the given resistance R_s and the scan rate v into eq 7, where $n = 1$, $T = 298$ K, $A = 0.26$ cm^2, $D_o = 7.1 \times 10^{-6}$ cm^2·s^{-1},[63] and $C_o = 5$ mM. The working curve obtained by plotting $H^{4/5}$ against ΔE_p is shown in Figure 7d, which clearly exhibits a linear dependence of $H^{4/5}$ on ΔE_p. The coincidence of $H^{4/5}$ vs ΔE_p curves at different scan rates indicates not only the reliability and stability of our system but also the fact that the $H-\Delta E_p$ relation is independent of the potential scan rate.

After the $H^{4/5}-\Delta E_p$ working curve is obtained, the $R_{t(app)}$ of the Au/AUT/AuNP electrode can be calculated according to the method described below. Taking, for example, the Au/AUT/AuNP electrode with a 20 min assembly time, we first obtain the values of ΔE_p at different scan rates from Figure 6a and then find the corresponding H values on the $H^{4/5}-\Delta E_p$ working curve shown in Figure 7d. Then for the Au/AUT/AuNP electrode with a 20 min assembly time, the variation of H as a function of $v^{1/2}$ is given by plotting H against $v^{1/2}$. For the other Au/AUT/AuNP samples, similar $H-v^{1/2}$ curves are obtained by the same method described above, and the results for all

Au/AUT/AuNP electrodes are shown in Figure 8. From Figure 8 two features are immediately apparent: (1) H increases linearly with increasing $v^{1/2}$. (2) The slope of the $H-v^{1/2}$ curve decreases as the assembly time is increased. According to eq 8, H is proportional to the square root of the scan rate, and the slope is a function of $R_{t(app)}$. As illustrated in Figure 8, the linear relation between H and $v^{1/2}$ for all Au/AUT/AuNP electrodes clearly demonstrates that the experimental results are in good agreement with the theoretical predictions. Furthermore, according to eq 8, the slope of the $H-v^{1/2}$ curve increases linearly as a function of $R_{t(app)}$; therefore, the decrease of the slope with increasing assembly time suggests that a longer assembly time results in a smaller $R_{t(app)}$. This is in line with the variation trend of the particle density as a function of the assembly time, because a larger particle density leads to more tunneling channels for Au/AUT/AuNPs and therefore a smaller apparent tunneling resistance $R_{t(app)}$. The $R_{t(app)}$ values calculated from the slopes in Figure 8 are 103.1, 35.2, 14.9, and 9.9 Ω, respectively, for assembly times of 20, 45, 480, and 1440 min. After normalization by a 0.26 cm^2 electrode area, the corresponding values of $R_{t(app,nor)}$ are 26.8, 9.2, 3.9, and 2.6 Ω·cm^2, respectively.

After obtaining the values of $R_{t(app,nor)}$, we can calculate the particle density N on the basis of eq 6, if we also know the tunneling resistance at a single AuNP ($R_{t(AuNP)}$). The AuNPs prepared by the Frens method[10] were coated by citrate ions, which have strong electrostatic interaction with positively charged amino groups on the AUT monolayer. This interaction leads to the immobilization of AuNPs on gold substrates. Therefore, one single tunneling route from the gold substrate to AuNPs contains two molecule layers: AUT and citrate. The tunneling thickness l corresponds to 15 methylene groups (11 methylene groups and 1 amino group from AUT and 3
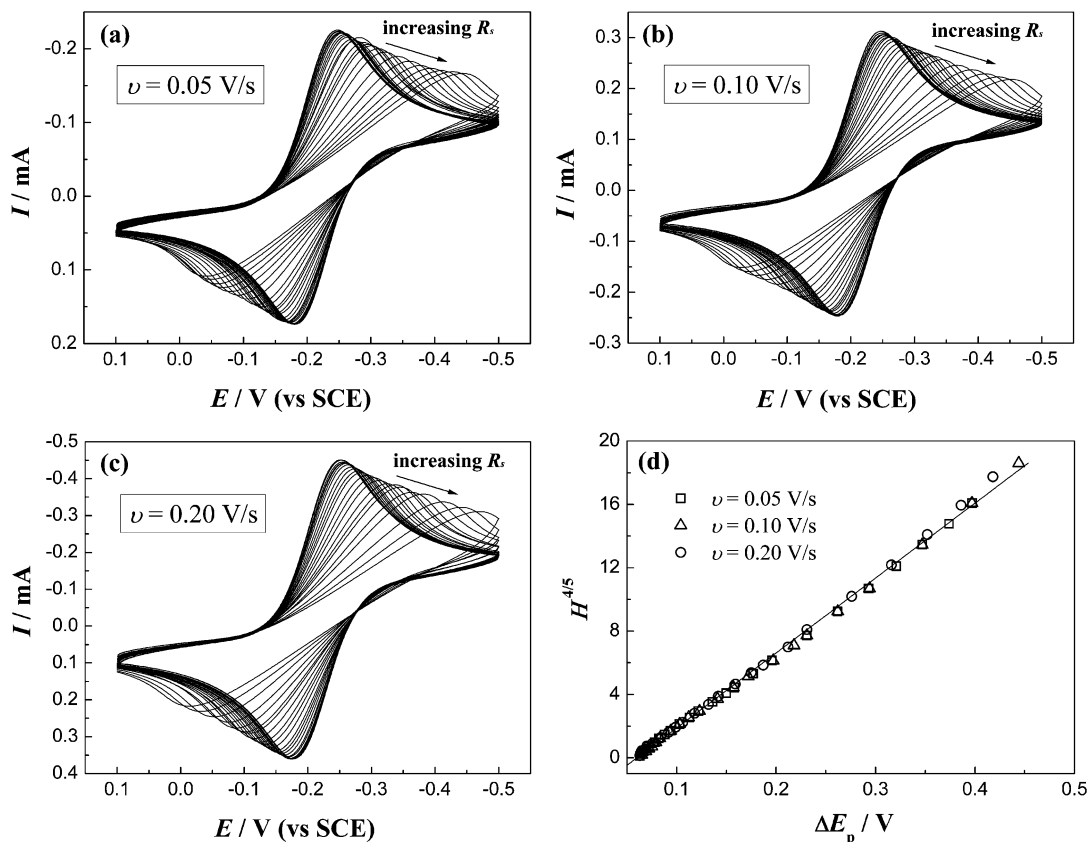
Figure 7. Cyclic voltammograms of the bare gold electrode with different given resistances in 5 mM $Ru(NH_3)_6Cl_3$ solution using 1 M KCl as the supporting electrolyte. Scan rate: (a) 0.05 $V \cdot s^{-1}$, (b) 0.1 $V \cdot s^{-1}$, (c) 0.2 $V \cdot s^{-1}$. The values of the given resistances are 2, 5, 8, 10, 15, 20, 30, 40, 50, 60, 80, 100, 120, 150, 180, 200, 250, 300, 400, 500, 600, 700, 800, 900, and 1000 Ω. (d) Working curve showing the variation of $H^{4/5}$ with ΔE_p.
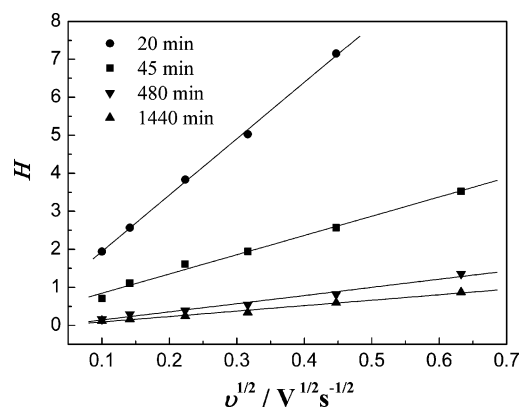

Figure 8. H vs $\upsilon^{1/2}$ plots of the Au/AUT/AuNP electrode with different assembly times. H values at different scan rates are obtained by first measuring ΔE_p in Figure 6 and then finding the corresponding H in the working curve shown in Figure 7d.

methylene groups from citrate[69]). For electron tunneling through two molecule layers, the tunneling coefficient β is 1.16 per methylene group.[55] The effective contact resistance of the two separated gold phases, R_0, was measured to be 18500 Ω using a Au/alkanethiol/Au structure.[54] On the basis of eq 4, R_t is calculated to be 6.67×10^{12} Ω, and therefore, the tunneling resistance for a single AuNP ($R_{t(AuNP)}$) is 2.22×10^{11} Ω according to eq 5.

After the values of $R_{t(app,nor)}$ and $R_{t(AuNP)}$ are obtained, N can be calculated on the basis of eq 6, and the results are shown in Figure 2f (open circles). It is clear from Figure 2f that the calculated value of N is in reasonable agreement with that

obtained from SEM images, implying that the apparent tunneling resistance is the dominant factor controlling the particle-dependent CV behavior. In addition, the consistence of the corresponding N values obtained by electrochemical and SEM measurements indicates that the theory of solution resistance is successfully employed to describe the apparent tunneling resistance of the Au/AUT/AuNP electrode. This is consistent with the results obtained at single-wall carbon nanotube array electrodes,[42] which were chemically assembled on a gold surface by AUT monolayers. However, Figure 2f (open circles) also demonstrates that the N values calculated from eq 6 deviate negatively from those obtained from SEM images, especially for the samples with a long incubation time in gold colloid. This observation is attributed to the fact that, at a high particle density, the $R_{t(app)}$ value is so small that it is of the same order of magnitude as real solution resistance. Therefore, the solution resistance cannot be omitted from the EQC shown in Figure 5c, and the $R_{t(app)}$ value calculated from the slopes in Figure 8 is the sum of $R_{t(app)}$ and the solution resistance. This also means that a high particle density (long assembly time) can greatly reduce the influence of electron tunneling on electrochemical behaviors. In fact, for the Au/AUT/AuNPs with assembly times of 480 and 1440 min, the ΔE_p values at a scan rate of 0.01 $V \cdot s^{-1}$ are 64 and 63 mV, respectively, implying that, at a low potential sweep rate, the tunneling process has little effect on the CV behavior for the sample with a very high particle density. Therefore, for the electroanalysis based on nanoparticle assembly electrodes, it is desirable to carry out measurements by applying a relatively slow potential sweep rate and employing electrodes with a high particle density.

Electrochemical Behavior of AuNP Assembly

J. Phys. Chem. C, Vol. 112, No. 17, 2008 **7045**

Conclusions

We have demonstrated that electron communication between the assembled AuNPs and the underlying gold substrate can occur though there is an insulating AUT monolayer sandwiched between them. The outer-sphere reversible redox couple $Ru(NH_3)_6^{3+/2+}$ exhibits quasi-reversible CV features at the Au/AUT/AuNP electrode, indicating that electron tunneling across the AUT monolayer plays a key role in dominating the whole electron-transfer rate. We also show that the particle density of Au/AUT/AuNP electrodes has a great effect on their electrochemical behaviors: briefly, the higher the particle density, the more reversible the CV behavior of AuNP assembly electrodes. We believe that the particle density exerts an influence on the CV features of Au/AUT/AuNPs by changing the number of tunneling channels between AuNPs and the gold substrate. A higher particle density leads to more tunneling channels, then a smaller apparent tunneling resistance, and still then more reversible CV behaviors. The apparent tunneling resistance of the Au/AUT/AuNPs reflects the tunneling probability across the insulating organic layer that immobilizes the AuNPs on the substrates. We have shown that the apparent tunneling resistance influences the CV behavior of Au/AUT/AuNPs in a way similar to that of the solution resistance. We demonstrate that the tunneling resistance can be quantitatively treated using the theory of solution resistance and can be employed to calculate the particle density. The calculated particle density is in reasonable agreement with that obtained from SEM images. This work provides solid evidence that the tunneling process across the bridging molecules has a great effect on the electrochemical behaviors of nanoparticle array electrodes. As a result, when assembled nanoparticle electrodes are used in electroanalytical works, the tunneling process must be taken into account, especially for the electrode with a relatively lower particle density.

Supporting Information Available: Calculation of the average center-to-center distance between adjacent particles. This material is available free of charge via the Internet at http://pubs.acs.org.

References and Notes

(1) Shipway, A. N.; Katz, E.; Willner, I. *ChemPhysChem* **2000**, *1*, 18−52.

(2) Shenhar, R.; Rotello, V. M. *Acc. Chem. Res.* **2003**, *36*, 549−561.

(3) Kovtyukhova, N. I.; Mallouk, T. E. *Chem.—Eur. J.* **2002**, *8*, 4355−4363.

(4) Zhang, H. F.; Hussain, I.; Brust, M.; Butler, M. F.; Rannard, S. P.; Cooper, A. I. *Nat. Mater.* **2005**, *4*, 787−793.

(5) Lahav, M.; Sehayek, T.; Vaskevich, A.; Rubinstein, I. *Angew. Chem., Int. Ed.* **2003**, *42*, 5575−5579.

(6) Yin, Y.; Lu, Y.; Gates, B.; Xia, Y. *J. Am. Chem. Soc.* **2001**, *123*, 8718−8729.

(7) Sastry, M.; Rao, M.; Ganesh, K. N. *Acc. Chem. Res.* **2002**, *35*, 847−855.

(8) Grabar, K. C.; Smith, P. C.; Musick, M. D.; Davis, J. A.; Walter, D. G.; Jackson, M. A.; Guthrie, A. P.; Natan, M. J. *J. Am. Chem. Soc.* **1996**, *118*, 1148−1153.

(9) Sugimura, H.; Nakagiri, N. *J. Am. Chem. Soc.* **1997**, *119*, 9226−9229.

(10) Frens, G. *Nat. Phys. Sci.* **1973**, *241*, 20.

(11) Sun, Y. G.; Xia, Y. N. *Science* **2002**, *298*, 2176−2179.

(12) Puntes, V. F.; Krishnan, K. M.; Alivisatos, A. P. *Science* **2001**, *291*, 2115−2117.

(13) Chemseddine, A.; Moritz, T. *Eur. J. Inorg. Chem.* **1999**, 235−245.

(14) Brown, K. R.; Walter, D. G.; Natan, M. J. *Chem. Mater.* **2000**, *12*, 306−313.

(15) Demers, L. M.; Park, S. J.; Taton, T. A.; Li, Z.; Mirkin, C. A. *Angew. Chem., Int. Ed.* **2001**, *40*, 3071−3073.

(16) Colvin, V. L.; Goldstein, A. N.; Alivisatos, A. P. *J. Am. Chem. Soc.* **1992**, *114*, 5221−5230.

(17) Musick, M. D.; Pena, D. J.; Botsko, S. L.; McEvoy, T. M.; Richardson, J. N.; Natan, M. J. *Langmuir* **1999**, *15*, 844−850.

(18) Grabar, K. C.; Brown, K. R.; Keating, C. D.; Stranick, S. J.; Tang, S. L.; Natan, M. J. *Anal. Chem.* **1997**, *69*, 471−477.

(19) Schmid, G.; Baumle, M.; Beyer, N. *Angew. Chem., Int. Ed.* **2000**, *39*, 181−183.

(20) Freeman, R. G.; Grabar, K. C.; Allison, K. J.; Bright, R. M.; Davis, J. A.; Guthrie, A. P.; Hommer, M. B.; Jackson, M. A.; Smith, P. C.; Walter, D. G.; Natan, M. J. *Science* **1995**, *267*, 1629−1632.

(21) Shipway, A. N.; Lahav, M.; Willner, I. *Adv. Mater.* **2000**, *12*, 993−998.

(22) Shipway, A. N.; Lahav, M.; Blonder, R.; Willner, I. *Chem. Mater.* **1999**, *11*, 13−15.

(23) Shipway, A. N.; Willner, I. *Chem. Commun.* **2001**, 2035−2045.

(24) Brown, K. R.; Fox, A. P.; Natan, M. J. *J. Am. Chem. Soc.* **1996**, *118*, 1154−1157.

(25) Diao, P.; Guo, M.; Hou, Q. C.; Xiang, M.; Zhang, Q. *J. Phys. Chem. B* **2006**, *110*, 20386−20391.

(26) Bharathi, S.; Nogami, M.; Ikeda, S. *Langmuir* **2001**, *17*, 1−4.

(27) Cheng, W.; Dong, S.; Wang, E. *Langmuir* **2002**, *18*, 9947−9952.

(28) Cheng, W.; Dong, S.; Wang, E. *Anal. Chem.* **2002**, *74*, 3599−3604.

(29) Jia, J.; Wang, B.; Wu, A.; Cheng, G.; Li, Z.; Dong, S. *Anal. Chem.* **2002**, *74*, 2217−2223.

(30) Bright, R. M.; Walter, D. G.; Musick, M. D.; Jackson, M. A.; Allison, K. J.; Natan, M. J. *Langmuir* **1996**, *12*, 810−817.

(31) Yu, A. M.; Liang, Z. J.; Cho, J. H.; Caruso, F. *Nano Lett.* **2003**, *3*, 1203−1207.

(32) Zhu, T.; Fu, X.; Mu, T.; Wang, J.; Liu, Z. *Langmuir* **1999**, *15*, 5197−5199.

(33) Chirea, M.; Garcia-Morales, V.; Manzanares, J. A.; Pereira, C.; Gulaboski, R.; Silva, F. *J. Phys. Chem. B* **2005**, *109*, 21808−21817.

(34) Porter, M. D.; Bright, T. B.; Allara, D. L.; Chidsey, C. E. D. *J. Am. Chem. Soc.* **1987**, *109*, 3559−3568.

(35) Finklea, H. O.; Hanshew, D. D. *J. Am. Chem. Soc.* **1992**, *114*, 3173−3181.

(36) Miller, C.; Cuendet, P.; Graetzel, M. *J. Phys. Chem.* **1991**, *95*, 877−886.

(37) Becka, A. M.; Miller, C. J. *J. Phys. Chem.* **1992**, *96*, 2657−2668.

(38) Diao, P.; Jiang, D. L.; Cui, X. L.; Gu, D. P.; Tong, R. T.; Zhong, B. *J. Electroanal. Chem.* **1999**, *464*, 61−67.

(39) Diao, P.; Guo, M.; Jiang, D. L.; Jia, Z. B.; Cui, X. L.; Gu, D. P.; Tong, R. T.; Zhong, B. *J. Electroanal. Chem.* **2000**, *480*, 59−63.

(40) Diao, P.; Guo, M.; Tong, R. T. *J. Electroanal. Chem.* **2001**, *495*, 98−105.

(41) Diao, P.; Liu, Z. F.; Wu, B.; Nan, X. L.; Zhang, J.; Wei, Z. *ChemPhysChem* **2002**, *3*, 898−901.

(42) Diao, P.; Liu, Z. F. *J. Phys. Chem. B* **2005**, *109*, 20906−20913.

(43) Gooding, J. J.; Wibowo, R.; Liu, J. Q.; Yang, W.; Losic, D.; Orbons, S.; Mearns, F. J.; Shapter, J. G.; Hibbert, D. B. *J. Am. Chem. Soc.* **2003**, *125*, 9006−9007.

(44) Patolsky, F.; Weizmann, Y.; Willner, I. *Angew. Chem., Int. Ed.* **2004**, *43*, 2113−2117.

(45) Sheeney-Haj-Khia, L.; Basnar, B.; Willner, I. *Angew. Chem., Int. Ed.* **2005**, *44*, 78−83.

(46) Su, L.; Gao, F.; Mao, L. Q. *Anal. Chem.* **2006**, *78*, 2651−2657.

(47) Ozoemena, K. I.; Nyokong, T.; Nkosi, D.; Chambrier, I.; Cook, M. J. *Electrochim. Acta* **2007**, *52*, 4132−4143.

(48) Takehara, K.; Takemura, H.; Ide, Y. *Electrochim. Acta* **1994**, *39*, 817−822.

(49) Thompson, D.; Collins, I. *J. Colloid Interface Sci.* **1992**, *152*, 197.

(50) Cui, X. D.; Primak, A.; Zarate, X.; Tomfohr, J.; Sankey, O. F.; Moore, A. L.; Moore, T. A.; Gust, D.; Harris, G.; Lindsay, S. M. *Science* **2001**, *294*, 571−574.

(51) Hicks, J. F.; Zamborini, F. P.; Murray, R. W. *J. Phys. Chem. B* **2002**, *106*, 7751−7757.

(52) Hicks, J. F.; Zamborini, F. P.; Osisek, A.; Murray, R. W. *J. Am. Chem. Soc.* **2001**, *123*, 7048−7053.

(53) Wold, D. J.; Frisbie, C. D. *J. Am. Chem. Soc.* **2000**, *122*, 2970−2971.

(54) Beebe, J. M.; Engelkes, V. B.; Miller, L. L.; Frisbie, C. D. *J. Am. Chem. Soc.* **2002**, *124*, 11268−11269.

(55) Wold, D. J.; Frisbie, C. D. *J. Am. Chem. Soc.* **2001**, *123*, 5549−5556.

(56) Engelkes, V. B.; Beebe, J. M.; Frisbie, C. D. *J. Am. Chem. Soc.* **2004**, *126*, 14287−14296.

Diao et al.

(57) Slowinski, K.; Chamberlain, R. V.; Miller, C. J.; Majda, M. *J. Am. Chem. Soc.* **1997**, *119*, 11910−11919.

(58) Giersig, M.; Mulvaney, P. *J. Phys. Chem.* **1993**, *97*, 6334−6336.

(59) Reller, H.; Kirowa-Eisner, E.; Gileadi, E. *J. Electroanal. Chem.* **1982**, *138*, 65−77.

(60) Amatore, C.; Saveant, J. M.; Tessier, D. *J. Electroanal. Chem.* **1983**, *147*, 39−51.

(61) Sabatani, E.; Rubinstein, I. *J. Phys. Chem.* **1987**, *91*, 6663−6669.

(62) Bard, A. J.; Faulkner, L. R. *Electrochemical Methods: Fundamentals and Applications*, 2nd ed.; John Wiley & Sons, Inc.: New York, 2001.

(63) Bard, A. J.; Crayston, J. A.; Kittlesen, G. P.; Varco Shea, T.; Wrighton, M. S. *Anal. Chem.* **1986**, *58*, 2321−2331.

(64) Saito, Y. *Rev. Polarogr.* **1968**, *15*, 177−189.

(65) Penner, R. M.; Heben, M. J.; Longin, T. L.; Lewis, N. S. *Science* **1990**, *250*, 1118−1121.

(66) Wold, D. J.; Haag, R.; Rampi, M. A.; Frisbie, C. D. *J. Phys. Chem. B* **2002**, *106*, 2813−2816.

(67) Nicholson, R. S. *Anal. Chem.* **1965**, *37*, 667−671.

(68) Nicholson, R. S. *Anal. Chem.* **1965**, *37*, 1351−1355.

(69) Kim, J. J.; Kim, S.-K.; Kim, Y. S. *J. Electroanal. Chem.* **2003**, *542*, 61−66.

How does the particle density affect the electrochemical behavior of gold nanoparticle assembly?

Peng Diao [a]*, Min Guo [b]*, Qi Zhang [a]

[a] Department of Applied Chemistry, School of Materials Science and Engineering, Beijing University of Aeronautics and Astronautics, Beijing 100083, People's Republic of China

[b] Department of Physical Chemistry, University of Science and Technology Beijing, Beijing 100083, People's Republic of China.

Supporting Information

If we assume that the particle density is N particle·cm^{-2} and the particles are uniformly dispersed on the substrate, the unit area of 1 cm^2 can be evenly divided into N small squares with each one containing a particle in its center, as shown in the following Figure S1. The side length of the small square can be easily figured out, which is $(1/N)^{1/2}$ cm. Because the distance between the centers of two adjacent squares is equal to the side length of the small squares, the center-to-center separation of two adjacent particles is $(1/N)^{1/2}$ cm.
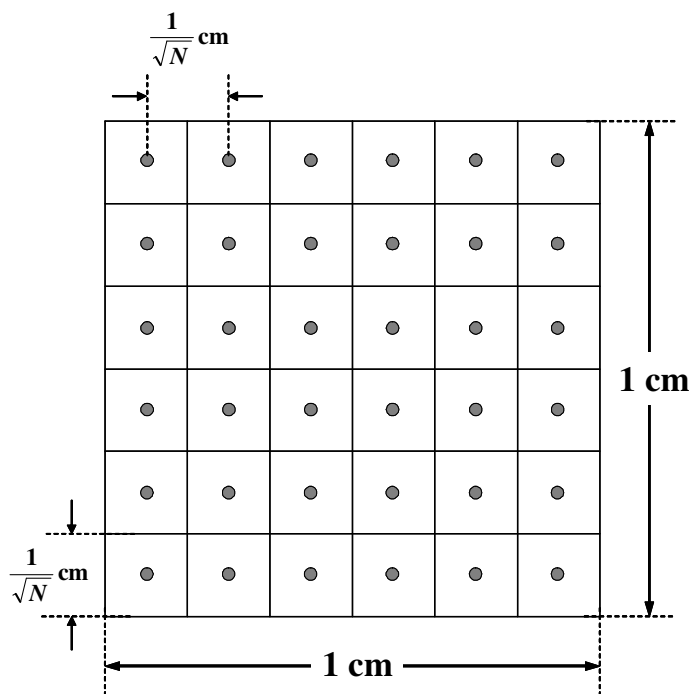

Figure S1. Schematic representation of the 1 cm^2 square divided into N small squares with each one containing a particle in its center.